Computers & Structures Vol. 35, No. 3, pp. 195–214, 1990
Printed in Great Britain.

0045-7949/90 $3.00 + 0.00
Pergamon Press plc

THREE-DIMENSIONAL NONLINEAR STATICS OF PIPELAYING USING CONDENSATION IN AN INCREMENTAL FINITE ELEMENT ALGORITHM

M. M. BERNITSAS and N. VLAHOPOULOS
Department of Naval Architecture and Marine Engineering, The University of Michigan, Ann Arbor, MI 48109, U.S.A.

(*Received* 9 *May* 1989)

Abstract—The problem of static, nonlinear three-dimensional deformation of pipelaying used in construction and installation of underwater pipelines is studied within the limits of small strain theory. The mathematical model consists of the pipeline model and geometric constraints imposed by the seabed and the lay vessel in stinger or J-type pipelaying. The pipeline is modeled as a thin-walled, slender, extensible or inextensible tubular beam–column. It is subject to gravity, lateral friction from the seabed, nonlinear three-dimensional deformation dependent hydrodynamic loads, torsion and distributed moments, varying axial tension, and internal and external static fluid forces. The problem is solved numerically by developing a nonlinear incremental finite element algorithm which features condensation and principles of contact mechanics. Condensation is used along with the geometric constraints to formulate a condensed problem which produces reaction forces. Strong nonlinearities present in the model are handled by an incremental finite element approach. The developed computer code is used to study stinger pipelaying for various stinger configurations, investigate the effect of water depth, and compare stinger to J-type pipelaying in deep water.

NOTATION

$\{AF\}$	constraint reaction force, exerted on the pipeline
A_i, A_o	inner and outer cross-sections of the pipeline, respectively
B	bending rigidity
C_D	drag coefficient
D_H	hydrodynamic diameter
E	modulus of elasticity
$\mathbf{F} = (F_1, F_2, F_3)$	internal force vector
H	torsional moment
H_i	x-coordinate of inner fluid free surface
H_W	x-coordinate of water free surface
$(\hat{i}, \hat{j}, \hat{k})$	triad of principal unit vectors
$[K]$	sum of the eight stiffness matrices appearing in eqn (33)
l, l_1	undeformed and deformed finite element length, respectively
$\mathbf{M} = (M_1, M_2, M_3)$	internal moment vector
m	external moment per unit length
$\hat{n}_c$	unit normal vector directed out of the infeasible domain
P_e	effective tension
$\mathbf{q}$	external force per unit length
$\mathbf{r}$	position vector for the pipeline centerline
$\mathbf{R}$	constraint reaction force exerted on the pipeline
s, s_1	arc length of the pipeline centerline measured in the initial unstrained state and deformed state, respectively
T	actual tension
$(\hat{t}, \hat{n}, \hat{b})$	triad of local principal unit vectors
$\hat{t}_c$	unit vector tangent to the stinger
$\mathbf{V}_n$	component of the relative flow velocity normal to the riser centerline
W	weight of the pipeline supported by the seabed
$(x_1, x_2, x_3) \equiv (x, y, z)$	coordinates of the pipeline's centerline
$(x_L, 0, z_L)$	coordinate of the stinger's lower end
$(x_U, 0, z_U)$	coordinate of the stinger's upper end

Greek symbols

Γ_c	contact region
Δ	incremental operator
δ	indicates correction at the reaction forces and displacements imposed by the constraints
ϵ_t	strain of the riser centerline in the tangential direction
κ	curvature defined by eqn (4)
μ_s	friction coefficient between seabed and pipeline
ρ_i	density of fluid inside the pipeline
ρ_w	density of water

Indices

c	indicates constrained degrees of freedom
f	indicates free degrees of freedom
l	indicates longitudinal degrees of freedom
t	indicates transverse degrees of freedom

Special symbols

$(\dot{})$	indicates the differential operator $\frac{d}{ds_1}$
${}^a[\,]_c^b$, ${}^a\{\,\}_c^b$	locations of indices a, b, c around a matrix or vector symbol represent the positions where the iteration number, i, the increment number, n, and the symbols of the type of degree of freedom are placed, respectively

1. INTRODUCTION

Underwater pipelines are subjected to high stresses during the installation process [1]. Thorough analysis of pipelaying is mandatory to ensure safe operation and minimal down time under specified environmental conditions [2]. Stinger and J-type pipelaying are the most common methods for construction and installation of pipelines. The former may be used at all water depths while the latter is exclusively used in deep waters. Both methods are studied in this paper.

Several numerical methods have been developed to solve the stinger pipelaying problem. Powers and Finn [1] used an initial value approach to analyze the small deflection static problem. In their finite element solution boundary conditions are assumed at the ocean floor and modified in an iterative procedure until boundary conditions at the lay vessel are satisfied. Ovunc and Mallareddy [3] solved the small deflection three-dimensional static problem using a stiffness matrix method. Wilkins [4] included nonlinear curvature in a finite difference two-dimensional static model. Gnone *et al.* [5, 6] compared experimental data to numerical predictions computed by a three-dimensional model that takes into consideration the geometric nonlinearity due to extension but neglects other geometric nonlinearities. Larsen and Kavlie [7] treated the two-dimensional, small deflection static problem by potential minimization. They neglected the geometric stiffness due to axial force and concentrated on resolving difficulties arising from modeling the seabed and stinger using springs. Konuk [8] solved a comprehensive, nonlinear, static, three-dimensional model for pipelines. Aspects of extensibility, deformation dependency of hydrodynamic loads, and implementation of constraints were not discussed. Experimental data were compared to numerical predictions produced by Suzuki and Jingu [9], using two-dimensional, small deflection, frequency domain analysis. Bryndum *et al.* [10] solved a linearized dynamic pipelaying problem using a finite difference scheme. Specified reaction coefficients were used to describe the unilateral constraints imposed by the seabed and stinger. Oliver and Onate [11] solved the static, small deflection, two-dimensional problem by a finite element approach. Constraints were imposed in an iterative scheme by prescribing nodal displacements where penetration occurred. In the present paper the static, three-dimensional, large deflection problem is studied. The pipeline is modeled, in Sec. 2, as a thin-walled, slender, extensible or inextensible, tubular beam–column, subject to gravity, tension, deformation dependent hydrodynamic loads, torsion, distributed moments, internal and external fluid static pressure, and seabed friction. In the solution algorithm, developed in Sec. 3, the load is applied incrementally in a finite element scheme. In each increment iteration is used for convergence and satisfaction of geometric constraints imposed by the seabed and stinger. In Sec. 4 the problems of stinger and J-type pipelaying are studied.

2. STATIC PIPELAYING MODEL

The mathematical model of pipelaying is comprised of the pipeline model and its boundary conditions, and geometric constraints imposed by seabed and stinger. It is assumed that the pipeline material is homogeneous, isotropic, and linearly elastic. Further, the following assumptions are made.

(i) Pipelines are thin-walled tubular columns.
(ii) Pipelines have circular cross-sections and are locally stiff so that plane sections remain plain after bending.
(iii) Shear deformation is neglected.
(iv) In the unloaded condition pipelines are assumed to be straight and free of structural imperfections.
(v) Pipelines are considered axially restrained at their lower end, and they may be extensible or inextensible.
(vi) The seabed is assumed to be flat and rigid.
(vii) The stinger is rigid with one end attached to the lay vessel. The stinger geometry is described by a quadratic polynomial.
(viii) Friction between seabed and pipeline is proportional to the weight of the pipeline supported by the seabed. The friction force is exerted in the y-direction (see Fig. 1).
(ix) There is no friction between the pipeline and the stinger.

Using the above assumptions we can develop a nonlinear three-dimensional mathematical model for static pipelaying following the model developed in [12] and [13] for tubular columns. The geometry of the pipeline axis is shown in Fig. 1 in the deformed configuration and symbols are explained in the Notation. Force and moment equilibria yield

$$\mathbf{F}' + \mathbf{q} = \mathbf{0} \tag{1}$$

and

$$\mathbf{M}' + (\hat{t} \times \mathbf{F}) + \mathbf{m} = \mathbf{0}, \tag{2}$$

where the internal force $\mathbf{F} = (F_1, F_2, F_3)$ and the internal moment $\mathbf{M} = (M_1, M_2, M_3)$. The constitutive equation for bending and torsion is

$$\mathbf{M} = B\kappa\hat{b} + H\hat{t}, \tag{3}$$

where $B = EI$ is bending rigidity, and H is torsional moment. $(\hat{t}, \hat{n}, \hat{b})$ is the triad of local principal unit vectors of the pipeline centerline

$$\hat{t} = \mathbf{r}', \quad \hat{b} = \mathbf{r}' \times \mathbf{r}''/\kappa, \quad \kappa = |\mathbf{r}''|. \tag{4}$$

Bold characters and "^" indicate vector and unit vector, respectively, and the differential operator

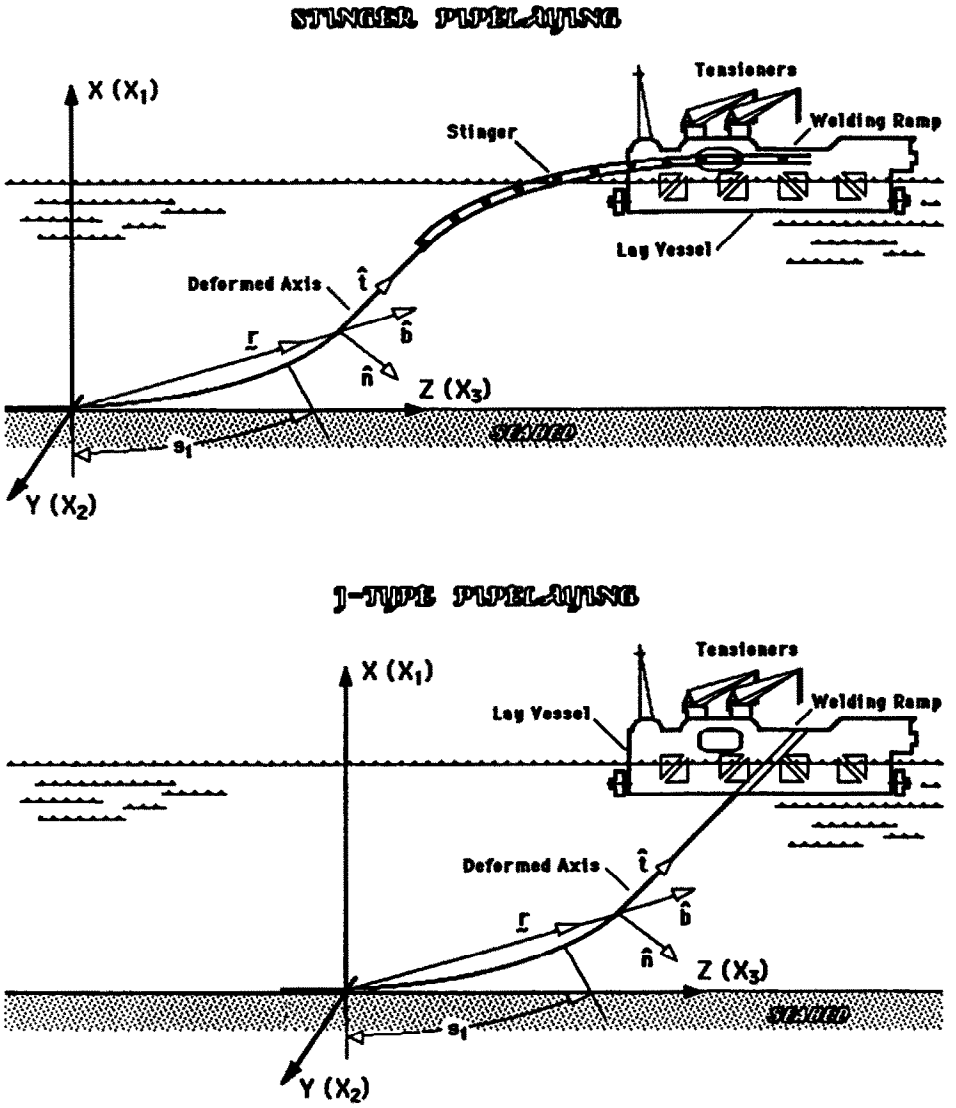

Fig. 1. Pipelaying.

d/ds_1 is with respect to the arc length s_1 of the deformed pipeline centerline. κ is the principal local curvature, and $\mathbf{r}$ is the position vector shown in Fig. 1:

$$\mathbf{r} = x_1\hat{i} + x_2\hat{j} + (x_3 + s)\hat{k}. \tag{5}$$

Combining eqns (1), (2), (3), and (4) we derive the governing equations for bending

$$-(B\mathbf{r}'')'' + [(P_e - B\kappa^2)\mathbf{r}']' + [H(\mathbf{r}' \times \mathbf{r}'')]' + (\mathbf{r}' \times \mathbf{m})' + \mathbf{q} = \mathbf{0} \tag{6}$$

and for torsion

$$H' + t \cdot \mathbf{m} = 0, \tag{7}$$

where s is the arc length of the pipeline centerline measured in the unstrained state and is related to s_1 by

$$\frac{ds_1}{ds} = 1 + \epsilon_t. \tag{8}$$

ϵ_t is the strain of the centerline in the tangential direction, defined as

$$\epsilon_t = \left|\frac{d\mathbf{r}}{ds} \cdot \frac{d\mathbf{r}}{ds}\right|^{1/2} - 1. \tag{9}$$

The actual tension T satisfies the constitutive equation

$$T = EA\epsilon_t, \tag{10}$$

where EA is stretching rigidity, and the actual tension

T is related to the effective tension P_e by

$$P_e = T + \rho_w g A_0[H_w - (x_1 + s)] - \rho_i g A_i[H_i - (x_1 + s)]. \quad (11)$$

H_w and H_i are the x coordinates of water and internal fluid free surfaces, ρ_w and ρ_i are the densities of water and internal fluid, $A_o = \pi D_o^2/4$ and $A_i = \pi D_i^2/4$, and $z = (x_1 + s)$ is measured from the pipeline lower end. P_e is the tangential component of the internal force $\mathbf{F}$

$$P_e = \mathbf{F} \cdot \hat{t}, \quad (12)$$

and $\mathbf{F}$ can be derived by integration of eqn (1). Since P_e is used in this formulation, the vertical component of $\mathbf{q}$ should include the effective riser weight per unit length W_e, defined as the weight of pipeline plus contents in water [12]. The hydrodynamic components of the external force q are

$$\mathbf{q}_H(s_1) = \begin{Bmatrix} q_{H_1} \\ q_{H_2} \\ q_{H_3} \end{Bmatrix} = \frac{1}{2} \rho_w C_D D_H |\mathbf{V}_n| \begin{Bmatrix} V_{n_1} \\ V_{n_2} \\ V_{n_3} \end{Bmatrix}, \quad (13)$$

where only the drag term is considered in the Morison–Borgman formula [14, 15], C_D is the drag coefficient, D_H is the hydrodynamic diameter, and $\mathbf{V}_n$ is the component of the relative flow velocity normal to the pipeline centerline. The following five boundary conditions must be defined:

(i) $\hat{t} \times \mathbf{M}$ or $\mathbf{r}'$ at $s_1 = 0$;
(ii) $\hat{t} \times \mathbf{M}$ or $\mathbf{r}'$ at the upper end;
(iii) $\mathbf{F}$ or $\mathbf{r}$ at $s_1 = 0$;
(iv) $\mathbf{F}$ or $\mathbf{r}$ at the upper end;
(v) the torsional moment at the lower or upper end.

To complete the mathematical model the geometric constraints imposed by the seabed and the stinger must be defined. The seabed, according to assumption (vi), is defined by the (y, z) plane as

$$x = 0. \quad (14)$$

The stinger geometry is defined by a second degree polynomial

$$x = az^2 + bz + c \quad (15)$$

and

$$y = 0 \quad (16)$$

$$x_L \le x \le x_U \quad (17)$$

$$z_L \le z \le z_U, \quad (18)$$

where $(x_L, 0, z_L)$, $(x_U, 0, z_U)$ are the coordinates of the lower and upper ends of the stinger. The upper end is located on the lay vessel. In addition, the value of a is specified. In the numerical applications discussed in Sec. 4, a is treated as a design parameter and its value is selected by minimizing the maximum equivalent stress in the pipeline.

The seabed and stinger impose nonpenetration and nonadhesion conditions on the pipeline which can be written, respectively, as

$$(\mathbf{r} - \mathbf{r}_c)\hat{n}_c \ge 0 \quad \text{on} \quad \Gamma_c \quad (19)$$

$$\mathbf{R} \cdot \hat{n}_c \ge 0 \quad \text{on} \quad \Gamma_c, \quad (20)$$

where $\mathbf{r}_c$ is the constraint position vector, $\hat{n}_c$ is the unit normal vector directed out of the infeasible domain, and $\mathbf{R}$ is the reaction force exerted on the pipeline. The nonfriction constraint for the stinger is

$$\hat{t}_c \cdot \mathbf{R} = 0, \quad (21)$$

where $\hat{t}_c$ is the unit tangent vector to the stinger. Finally, the friction constraint for the seabed is

$$|R_y| \le \mu_y \cdot W, \quad (22)$$

where R_y is the y-component of the force exerted on the pipeline, W is the weight of the pipeline supported by the seabed, and μ_y is the friction coefficient.

3. SOLUTION METHOD

The static pipelaying model developed in the previous section defines a three-dimensional, large deformation contact problem. A load incremental algorithm is developed to treat the nonlinearities and is described in Sec. 3.1. A condensation algorithm is developed in Sec. 3.2 which reduces the pipelaying problem to a condensed finite element problem based on the contact constraints. This method is different from other methods developed to solve similar contact problems. Hughes *et al.* [16] used Lagrangian multipliers and developed contact elements. Talaslidis and Panagiotopoulos [17] formulated the contact problem in a variational inequality form and solved it using standard quadratic optimization algorithms. Mahmoud *et al.* [18] developed an incremental solution scheme for two linear elastic bodies in contact and subjected to external loads. In their method, once contact is established in a boundary region by incremental load application, this boundary is assumed to remain in contact throughout the application of the entire load. In each increment the contact region is extended until equilibrium is established. In the condensation algorithm developed in this work to solve the static pipelaying problem, contact is not necessarily advancing as the incrementally applied load increases. Contact may regress depending on the stinger configuration. Stein and Wriggers [19] developed an updated Lagrangian formulation for a finite element computation of defor-

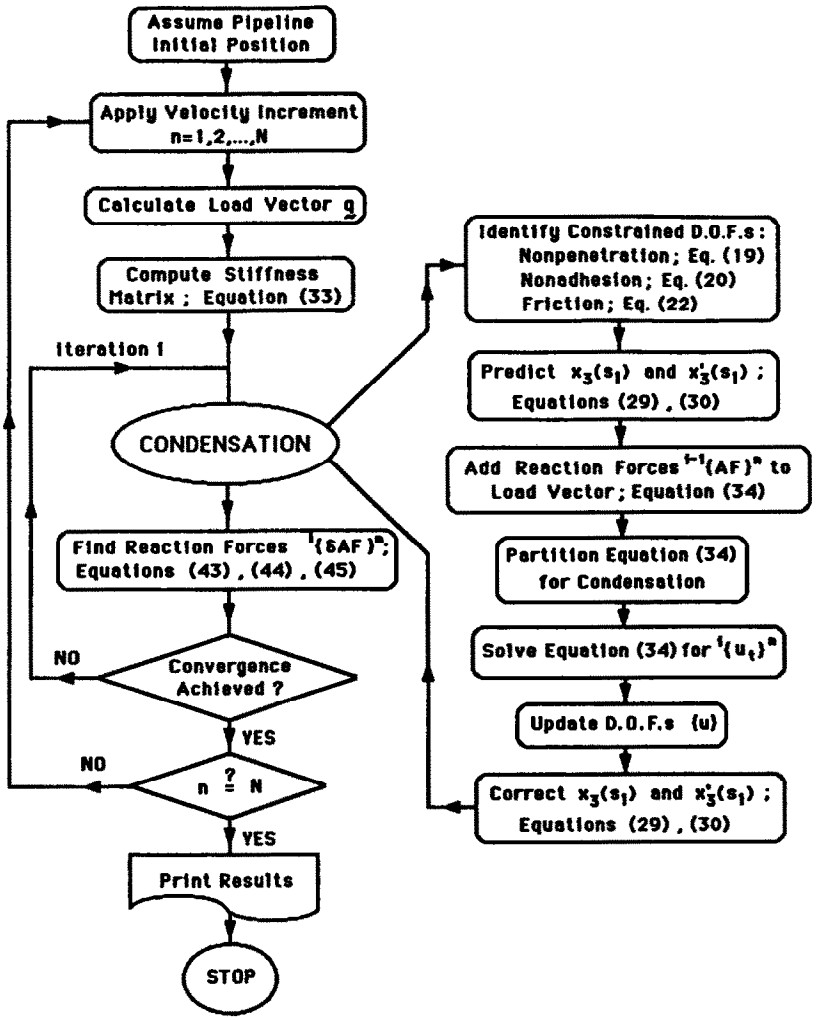

Fig. 2. Solution algorithm: load increments and condensation.

mation of rods with unilateral frictionless constraints. In each step the load increment is modified to allow for the new nodes that come in contact to just touch the constraint. Yagawa and Hirayama [20] developed special purpose contact elements inserted between surfaces to account for contact conditions. Gu [21] studied the problem of an elastic beam bent on a rigid barrier. He developed an incremental finite element algorithm with an interface equation to pinpoint the location of the moving and unknown marginal nodes separating the contact and noncontact regions. In contact regions the displacement was considered known, and a fixed number of elements was used to analyze the remaining unconstrained part of the beam. Karacostas *et al.* [22] studied the dynamic behavior of a submarine cable constrained by a frictionless, rigid seabed. Space and time discretization produced a unilateral contact problem which was formulated as a sequence of variational inequality problems. The latter were solved by quadratic programming.

3.1. *Load incremental algorithm*

The gravity loads, the fluid flow velocity, and hence the hydrodynamic load, are applied incrementally (see Fig. 2). Within each increment, iterations are performed until convergence of degrees of freedom is achieved. Within each iteration condensation is performed based on the contact constraints. The incremental counterpart of the mathematical model developed in Sec. 2 consists of the following equations. The weak incremental form of bending equation (6) is [23]

$$B\int_0^{l_1}\Delta\mathbf{r}''\cdot\bar{\mathbf{r}}''\,ds_1+(P_e-B\kappa^2)\int_0^{l_1}\Delta\mathbf{r}'\cdot\bar{\mathbf{r}}'\,ds_1$$

$$+\int_0^{l_1}(\mathbf{F}\cdot\Delta\mathbf{r}')(\mathbf{r}'\cdot\bar{\mathbf{r}}')\,ds_1$$

$$-2B\int_0^{l_1}(\mathbf{r}'\cdot\Delta\mathbf{r}'')(\mathbf{r}''\cdot\bar{\mathbf{r}}')\,ds_1$$

$$+H\int_0^{l_1}(\Delta\mathbf{r}'\times\mathbf{r}'')\cdot\bar{\mathbf{r}}'\,ds_1$$

$$+H\int_0^{l_1}(\mathbf{r}'\times\Delta\mathbf{r}'')\cdot\bar{\mathbf{r}}'\,ds_1+\int_0^{l_1}(\Delta\mathbf{r}'\times\mathbf{m})\bar{\mathbf{r}}'\,ds_1$$

$$+\int_0^{l_1}[\Delta\mathbf{r}'\times(\mathbf{m}_c^b\,\delta(s_1)+\mathbf{m}_c^t\,\delta(l_1-s_1))]\cdot\bar{\mathbf{r}}'\,ds_1$$

$$=\int_0^{l_1}[\Delta\mathbf{q}\times\Delta A\,\mathbf{q}_c^b\,\delta(s_1)+\Delta A\,\mathbf{q}_c^t\,\delta(l_1-s_1)]\cdot\bar{\mathbf{r}}\,ds_1$$

$$-\int_0^{l_1}(\Delta\mathbf{F}\cdot\mathbf{r}')(\mathbf{r}'\cdot\bar{\mathbf{r}}')\,ds_1-\Delta\mathbf{H}\int_0^{l}(\mathbf{r}'\times\mathbf{r}'')\cdot\bar{\mathbf{r}}'\,ds_1$$

$$-\int_0^{l_1}[\mathbf{r}'\times(\Delta\mathbf{m}+\Delta\mathbf{m}_c^b\delta(s_1)$$

$$+\Delta\mathbf{m}_c^t\,\delta(l_1-s_1))]\cdot\bar{\mathbf{r}}'\,ds_1$$

$$+\Delta\mathbf{F}\cdot\bar{\mathbf{r}}\Big|_0^{l_1}+B\Delta\mathbf{r}''\cdot\bar{\mathbf{r}}'\Big|_0^{l_1}. \tag{23}$$

The incremental form of torsion equation (7) is

$$\Delta\mathbf{H}(s_1)=\Delta\mathbf{H}(0)=\int_0^{s_1}\Delta\hat{t}\cdot\left(\mathbf{m}+\sum_{e=1}^{e_{s_1}}\mathbf{m}_e\cdot\delta(s_e-s_1)\right)ds_1-\int_0^{s_1}t\cdot\left(\Delta\mathbf{m}+\sum_{e=1}^{e_{s_1}}\Delta\mathbf{m}_e\cdot\delta(s_e-s_1)\right)ds_1. \tag{24}$$

The incremental form of the force equilibrium equation (1) is

$$\Delta\mathbf{F}=\Delta\mathbf{F}(l_1)-\int_{s_1}^{l_1}\left(\Delta\mathbf{q}+\sum_{k=k_{s_1}}^{k_{l_1}}\Delta A\,\mathbf{q}\,\delta(s_k-s_1)\right)ds_1. \tag{25}$$

The incremental forms of eqns (10), (11) and (12), respectively, are

$$\Delta P_e=EA\,\Delta\epsilon_t-\Delta x_1 g(\rho_w A_0-\rho_m A_i) \tag{26}$$

$$\Delta P_e=\Delta F_1 x_1'+\Delta F_2 x_2'+\Delta F_3\left(x_3'+\frac{1}{1+\epsilon_t}\right)+F_1\Delta x_1'+F_2\Delta x_2'+F_3\Delta x_3'-F_3\frac{\Delta\epsilon_t}{(1+\epsilon_t)^2} \tag{27}$$

$$\Delta T=\Delta\mathbf{F}\cdot\mathbf{r}'+\mathbf{F}\cdot\Delta\mathbf{r}'. \tag{28}$$

In the above equations, $\bar{\mathbf{r}}$ is the virtual displacement vector; l and l_1 are the undeformed and deformed element lengths. Further, $\mathbf{m}_c^b$ and $\mathbf{m}_c^t$ are the vectors of concentrated moments at the bottom and top of a finite element: $A\mathbf{q}_c^b$ and $A\mathbf{q}_c^t$ are the vectors of additional concentrated forces due to constraints at the bottom and top of a finite element; k_{s_1} and e_{s_1} are the total numbers of constrained nodes and concentrated moments, respectively, from the bottom of the pipeline up to s_1; s_k and s_e are the locations of constrained nodes and nodes with concentrated moments, respectively. It should be pointed out that in eqn (23) all quantities appearing in front of the integrals are considered constant for each element. In the above incremental formulation, the following equations are used to compute x_3, x_3', Δx_3, $\Delta x_3'$ in a prediction–correction scheme

$$x_3=x_3(0)+\int_0^{s_1}x_3'\,ds_1 \tag{29}$$

$$x_3'=(1-x_2'^2-x_1'^2)^{1/2}-\frac{1}{1+\epsilon_t} \tag{30}$$

$$\Delta x_3=\int_0^{s_1}\Delta x_3'\,ds_1 \tag{31}$$

$$\Delta x_3'=\left[1+\frac{F_3}{EA(1+\epsilon_t)^2}\right]\left[-\frac{x_2'\Delta x_2'+x_1'\Delta x_1'}{x_3'+\frac{1}{1+\epsilon_t}}+\frac{1}{EA(1+\epsilon_t)^2+F_3}\left[\Delta F_1 x_1'+\Delta F_2 x_2'+\Delta F_3\cdot\left(x_3'+\frac{1}{1+\epsilon_t}\right)+F_1\Delta x_1'+F_2\Delta x_2'-\Delta x_1 g(\rho_m A_i-\rho_w A_0)\right]\right]. \tag{32}$$

Thus, the number of degrees of freedom per element is reduced from 12 to eight. The resulting incremental finite element form is

$$\left(\sum_{l=1}^{8}[K_l]\right)\{u\}=\{F\}+\{AF\}, \tag{33}$$

where $\{u\}$ is the deformation vector due to the external force vector $\{F\}$ and force vector $\{AF\}$ due to the constraint reaction forces. The lth matrix is derived from the lth integral on the left hand side of eqn (23).

All stiffness matrices and, in general, the hydrodynamic load, are deformation dependent. Iterations are performed in each increment until convergence of degrees of freedom is achieved. An iterative procedure with predictor and corrector phases is used in each increment and all stiffness matrices, the equivalent nodal forces and the boundary conditions are updated. In the prediction phase, x_3, x_3', Δx_3, $\Delta x_3'$ are computed using eqns (29)–(32). In the correction

phase, $x_1, x_1', \Delta x_1, \Delta x_1', x_2, x_2', \Delta x_2, \Delta x_2'$ are computed by solving matrix equation (33), and $x_3, x_3', \Delta x_3, \Delta x_3'$ are corrected using eqns (29)–(32). The above algorithm is summarized in Fig. 2.

3.2. *Condensed problem*

With iteration i, in increment n, the nonadhesion and nonpenetration conditions given by eqns (19) and (20) are used to produce a condensed problem for the constrained degrees of freedom only. The latter are determined based on the following criteria.

(i) All y-degrees of freedom along the stinger satisfy eqn (16) and are constrained.
(ii) All x-degrees of freedom along the pipeline are constrained if the nonpenetration inequality condition (19) is violated.
(iii) If inequality (19) is violated by a node for the first time in the current iteration, no reaction force is available. Otherwise, the reaction force has been computed in the previous iteration/increment; in such case the nonadhesion inequality condition (20) is tested. If it is satisfied, contact is maintained through the current iteration; if not the node is released.
(iv) For all nodes that are in contact with the seabed, the friction inequality constraint (22) is tested. If it is satisfied the corresponding y-degree of freedom is constrained; otherwise it is released.

In the ith iteration of the nth increment the governing matrix equation is

$$[K]^n\, {}^i(u)^n = {}^i\{F\}^n + {}^{i-1}\{AF\}^n, \tag{34}$$

where $[K]^n$ is the stiffness matrix updated at the nth increment, and ${}^i\{u\}^n$, ${}^i(F)^n$ and ${}^{i-1}\{AF\}^n$ are incremental degrees of freedom, external forces, and reaction forces of the values of all increments.

Partitioning eqn (34) into constrained (c) and free (f) degrees of freedom we have

$$\begin{bmatrix} [K]_{cc} & [K]_{cf} \\ [K]_{fc} & [K]_{ff} \end{bmatrix}^n {}^i\begin{Bmatrix} \{u\}_c \\ \{u\}_f \end{Bmatrix}^n = {}^i\begin{Bmatrix} \{F\}_c \\ \{F\}_f \end{Bmatrix}^n + {}^{i-1}\begin{Bmatrix} \{AF\}_c \\ \{AF\}_f \end{Bmatrix}^n. \tag{35}$$

Indicating degrees of freedom in directions x_1 and x_2 by t (for transverse) and in direction x_3 by l (for longitudinal), we further partition eqn (35) as

$$\left[\begin{array}{cc|cc} [K_{tt}]_{cc} & [K_{tl}]_{cc} & [K_{tt}]_{cf} & [K_{tl}]_{cf} \\ [K_{lt}]_{cc} & [K_{ll}]_{cc} & [K_{lt}]_{cf} & [K_{ll}]_{cf} \\ \hline [K_{tt}]_{fc} & [K_{tl}]_{fc} & [K_{tt}]_{ff} & [K_{tl}]_{ff} \\ [K_{lt}]_{fc} & [K_{ll}]_{cc} & [K_{lt}]_{ff} & [K_{ll}]_{ff} \end{array}\right]^n \times {}^i\begin{Bmatrix} \{u_t\}_c \\ \{u_l\}_c \\ \hline \{u_t\}_f \\ \{u_l\}_f \end{Bmatrix}^n = {}^i\begin{Bmatrix} \{F_t\}_c \\ \{F_l\}_c \\ \hline \{F_t\}_f \\ \{F_l\}_f \end{Bmatrix}^n + {}^{i-1}\begin{Bmatrix} \{AF_t\}_c \\ \{AF_l\}_c \\ \hline \{AF_t\}_f \\ \{AF_l\}_f \end{Bmatrix}^n, \tag{36}$$

where

$${}^i\begin{Bmatrix} \{u_t\}_c \\ \{u_l\}_c \\ \{u_t\}_f \\ \{u_l\}_f \end{Bmatrix}^n \equiv {}^i\begin{Bmatrix} \begin{Bmatrix} x_1 \\ x_2 \\ x_3 \end{Bmatrix}_c \\ \begin{Bmatrix} x_1 \\ x_2 \\ x_1 \\ x_2 \end{Bmatrix}_f \\ \begin{Bmatrix} x_3 \\ x_3 \end{Bmatrix}_f \end{Bmatrix}^n \tag{37}$$

$${}^i\begin{Bmatrix} \{F_t\}_c \\ \{F_l\}_c \\ \{F_t\}_f \\ \{F_l\}_f \end{Bmatrix}^n \equiv {}^i\begin{Bmatrix} \begin{Bmatrix} F_1 \\ F_2 \\ F_3 \end{Bmatrix}_c \\ \begin{Bmatrix} F_1 \\ F_2 \\ M_1 \\ M_2 \end{Bmatrix}_f \\ \begin{Bmatrix} F_3 \\ M_3 \end{Bmatrix}_f \end{Bmatrix}^n \tag{38}$$

$${}^{i-1}\begin{Bmatrix} \{AF_t\}_c \\ \{AF_l\}_c \\ \{AF_t\}_f \\ \{AF_l\}_f \end{Bmatrix}^n \equiv {}^{i-1}\begin{Bmatrix} \begin{Bmatrix} AF_1 \\ AF_2 \\ AF_3 \end{Bmatrix}_c \\ \begin{Bmatrix} AF_1 \\ AF_2 \\ AM_1 \\ AM_2 \end{Bmatrix}_f \\ \begin{Bmatrix} AF_3 \\ AM_3 \end{Bmatrix}_f \end{Bmatrix}^n \tag{39}$$

$${}^{i-1}\begin{Bmatrix} \{AF_t\}_c \\ \{AF_l\}_c \end{Bmatrix}^n = {}^{i-1}\begin{Bmatrix} \begin{Bmatrix} AF_1 \\ AF_2 \\ AM_1 \\ AM_2 \end{Bmatrix}_f \\ \begin{Bmatrix} AF_3 \\ AM_3 \end{Bmatrix}_f \end{Bmatrix}^n = \{0\}. \tag{40}$$

Eliminating the longitudinal degrees of freedom (x_3, x_3') from eqn (36), using eqns (29)–(32), we derive the following matrix equation for the transverse degrees of freedom:

$$\begin{bmatrix} [K_{tt}]_{cc} & [K_{tt}]_{cf} \\ [K_{tt}]_{fc} & [K_{tt}]_{ff} \end{bmatrix}^n {}^i\begin{Bmatrix} \{u_t\}_c \\ \{u_t\}_f \end{Bmatrix}^n = {}^i\begin{Bmatrix} \{F_t\}_c \\ \{F_t\}_f \end{Bmatrix}^n + {}^{i-1}\begin{Bmatrix} \{AF_t\}_c \\ \{AF_t\}_f \end{Bmatrix}^n. \tag{41}$$

Advancing from iteration i to $(i+1)$ in increment n, results in changes to the incremental displacement vector ${}^{i}\{u\}^{n}$ and the additional reaction force vector ${}^{i}\{\delta AF\}^{n}$. Thus, we have

$$\begin{bmatrix}[K_{tt}]_{cc} & [K_{tt}]_{cf}\\ [K_{tt}]_{fc} & [K_{tt}]_{ff}\end{bmatrix}^{n} {}^{i}\begin{Bmatrix}\{\delta u_t\}_c\\ \{\delta u_t\}_f\end{Bmatrix}^{n} = {}^{i}\begin{Bmatrix}\{\delta AF_t\}_c\\ \{\delta AF_t\}_f\end{Bmatrix}^{n}. \quad (42)$$

Since ${}^{i}\{\delta AF_t\}_f^n = \{0\}$, eqn (42) can be condensed to

$$([K_{tt}]_{cc}^{n} - [K_{tt}]_{cf}^{n}[K_{tt}]_{ff}^{n-1}[K_{tt}]_{fc}^{n})^{i}\{\delta u_t\}_c^n = {}^{i}\{\delta AF_t\}_c^n, \quad (43)$$

where ${}^{i}\{\delta u_t\}_c^n$ is computed from the following equation, using the geometry of the constraint $\{u_c\}$ and the values of the incremental displacement vectors computed in the previous increments and the last iteration

$${}^{i}\{\delta u_t\}_c^n = \{u_c\} - \sum_{j=1}^{n-1}\{u_t\}_c^i - {}^{i}\{u_t\}_c^n. \quad (44)$$

Further, the nonfriction constraint of the stinger as expressed by eqn (21) yields

$$\hat{t}\cdot \mathbf{AF}_c = t_1\cdot AF_{c_1} + t_2\cdot AF_{c_2} + t_3\cdot AF_{c_3} = 0, \quad (45)$$

from which AF_{c_3} can be computed.

4. APPLICATIONS

The algorithm developed in the previous section to solve the pipelaying problem formulated in Sec. 2 has been implemented in program PIPELAY.NS.3D (*PIPE*line *LAY*ing *N*onlinear *S*tatic 3-*D*imensional Analysis). A major task in developing algorithms for nonlinear structural analysis is verification of the computer code. Our approach to verification is described in Sec. 4.1. In the rest of this section several numerical applications are used to study stinger pipelaying in moderate and deep water, and J-type pipelaying in deep water.

4.1. *Verification*

The major functions of program PIPELAY.NS.3D which must be verified are as follows.

(i) The solution algorithm for the three-dimensional, large deformation, nonlinear analysis of the pipeline.
(ii) The algorithm for identifying constrained degrees of freedom using the nonpenetration and nonadhesion conditions, and the friction constraint on the seabed boundary.
(iii) The condensation and solution process.

The first function of the program has been tested thoroughly over a period of six years by systematic comparison with linear programs and simple nonlinear applications that can be solved analytically [12]. The ability of PIPELAY.NS.3D to handle the extensibility of beam–column structures has also been tested for short stiff beams [13].

The second function of the program has been tested in the following ways.

(i) The entire pipeline was laid incrementally on a flat seabed under the action of its own weight. It was verified that all nodal points, including the two boundary points, were in contact with the seabed. The reaction forces were all equal and their sum was equal to the total pipeline weight in water. The nodal bending moments were almost equal to zero.
(ii) The entire pipeline was laid to a flat seabed and was subjected to lateral horizontal uniform load. The friction coefficient was given different values and the pipeline deflection was verified to be compatible with the friction force.
(iii) In all application cases all constraint conditions defined by eqns (14)–(21) were satisfied.

The third function of the program, condensation, has been tested in various substructuring applications. A substructuring-condensation process was developed in solving the problem of nonlinear, large deflection, three-dimensional, static and dynamic analyses of nonintegral riser bundles [23, 24]. Further, it was verified that all degrees of freedom identified as constrained in the following pipelaying applications were the only degrees of freedom present in the condensed matrix form [eqn (43)].

4.2. *Stinger pipelaying*

In this subsection, two stinger pipelaying applications, in moderate water depth, are considered. The properties of the pipeline used in all numerical applications in this paper are summarized in Table 1. A heavy coating is added to the pipeline to keep it in place after installation [2]. The external diameter of coating and density are also shown in Table 1.

The first application in this section involves pipelaying in 67 m water depth, in a tidal current of surface velocity 1.0 m/sec. The current velocity is in the z-direction and the pipelaying bending is planar in the (x, z) plane. The stinger end point coordinates are $(x_U, z_U) = (72.0, 400.0\text{ m})$ for the upper end, and $(x_L, z_L) = (41.5, 265.0\text{ m})$ for the lower end. These coordinates are used to define coefficients b and c in terms of a in eqn (15). Coefficient a is used as a design

Table 1. Properties of pipeline used in numerical applications

Property	Value
External diameter, D_0	0.61 m
Internal diameter, D_i	0.58 m
Diameter of coating, D_c	0.71 m
Density of steel pipes, ρ_{st}	7900 kg/m^3
Density of water, ρ_0	1025 kg/m^3
Density of coating, ρ_c	3000 kg/m^3
Tension applied at the pipeline's upper end	580 kN

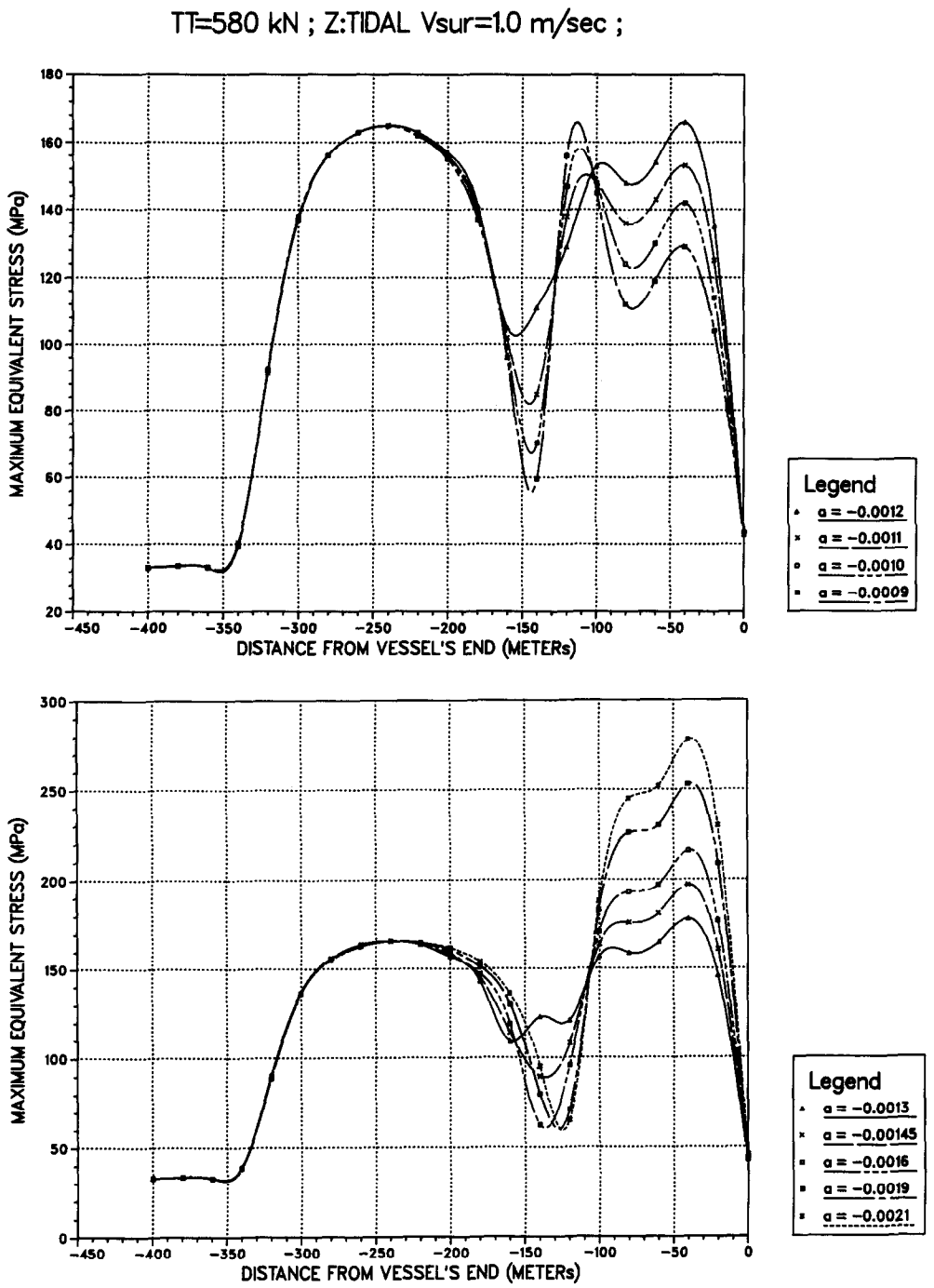

Fig. 3. Maximum equivalent for two-dimensional pipelaying in 67 m water depth; nine stinger configurations.

parameter as shown in Fig. 3, to find a good stinger design. No attempt is made to optimize for a. The value of $a = -0.0012$ selected, however, is expected to be very close to the actual optimum. The two maxima appearing in the maximum equivalent stress graph—one along the unsupported part of the pipeline and the other along the stinger supported section of the pipeline—are almost equal for the selected value of a. The maximum equivalent stress is defined as the maximum equivalent von Mises stress in any particular cross-section of the pipeline. The corresponding lateral deflection is shown in Fig. 4.

In the second application the tidal current is applied in the y-direction, thus making the pipeline's deflection three-dimensional as shown in Fig. 6 for $a = -0.0012$. The latter was selected by comparing the maximum equivalent stress in the pipeline for the various values of a shown in Fig. 5.

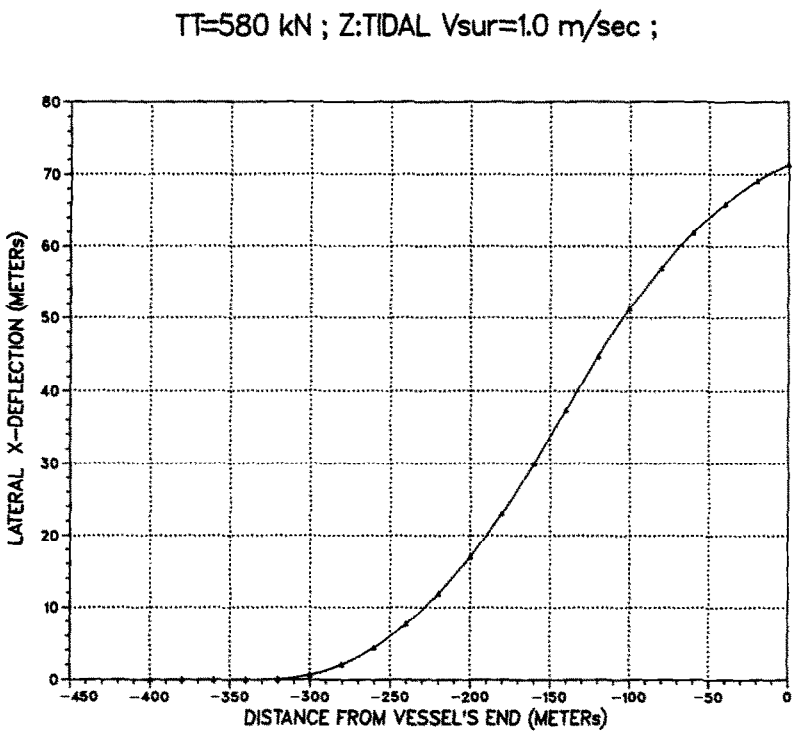

Fig. 4. Inplane pipeline deflection for two-dimensional pipelaying in 67 m water depth; stinger configuration $a = -0.0012$.

4.3. *Deep water stinger pipelaying*

Two applications similar to those considered in the previous section are studied in 125 m water depth. The stinger geometry is defined by eqn (15) and the following coordinates of the upper and lower stinger ends, respectively: $(x_U, z_U) = (128.0, 440.0\,\text{m})$ and $(x_L, z_L) = (78.0, 305.0\,\text{m})$. On the basis of the maximum equivalent stress graphs shown in Figs 7 and 9, the value of $a = -0.0011$ was selected. The corresponding deflections for two-dimensional and three-dimensional cases are shown in Figs 8 and 10, respectively.

4.4. *Deep water J-type pipelaying*

In deep water the alternative pipelaying method, J-type, may be used. The pipeline is laid without stinger support at a much sharper angle at the lay vessel. This is shown in the two- and three-dimensional applications in Figs 11 and 12, respectively. In J-type pipelaying the maximum equivalent stress exhibits one peak along the unsupported pipeline section.

4.5. *Conclusions*

By studying the numerical application results shown in Figs 3–12, the following conclusions can be drawn.

(i) In stinger pipelaying, stresses along the pipeline section which remains in contact with the stinger are the same in two- and three-dimensional applications. This is so because the pipeline deflection is restricted by the stinger in both the (x, z) plane and the y-direction.

(ii) In static analysis, the major load component exerted on the pipeline is due to the pipeline weight in water and not the hydrodynamic load. Thus, the difference between stresses in two- and three-dimensional cases diminishes as the water depth increases. This can be concluded by comparing Fig. 3 to Fig. 5, Fig. 7 to Fig. 9, and Fig. 11 to Fig. 12.

(iii) In stinger pipelaying two peaks appear in the maximum equivalent stress graphs, as shown in Figs 3, 5, 7 and 9. A good stinger configuration should make the two maxima, one located in the unsupported pipeline section and the other in the stinger supported section, nearly equal, so that the latter is not subjected to extensive stress.

(iv) In deeper water, the unsupported pipeline length is longer, and the touch down point is further away from the lay vessel. This becomes obvious by comparing Figs 4 and 6 to Figs 8 and 10.

(v) In stinger pipelaying, stresses increase with water depth because of the increase in length of the unsupported pipeline section (compare Figs 3 and 5 to 7 and 9, respectively).

(vi) In stinger pipelaying, the geometry of the stinger dominates the stress distribution along the stinger supported section of the pipe.

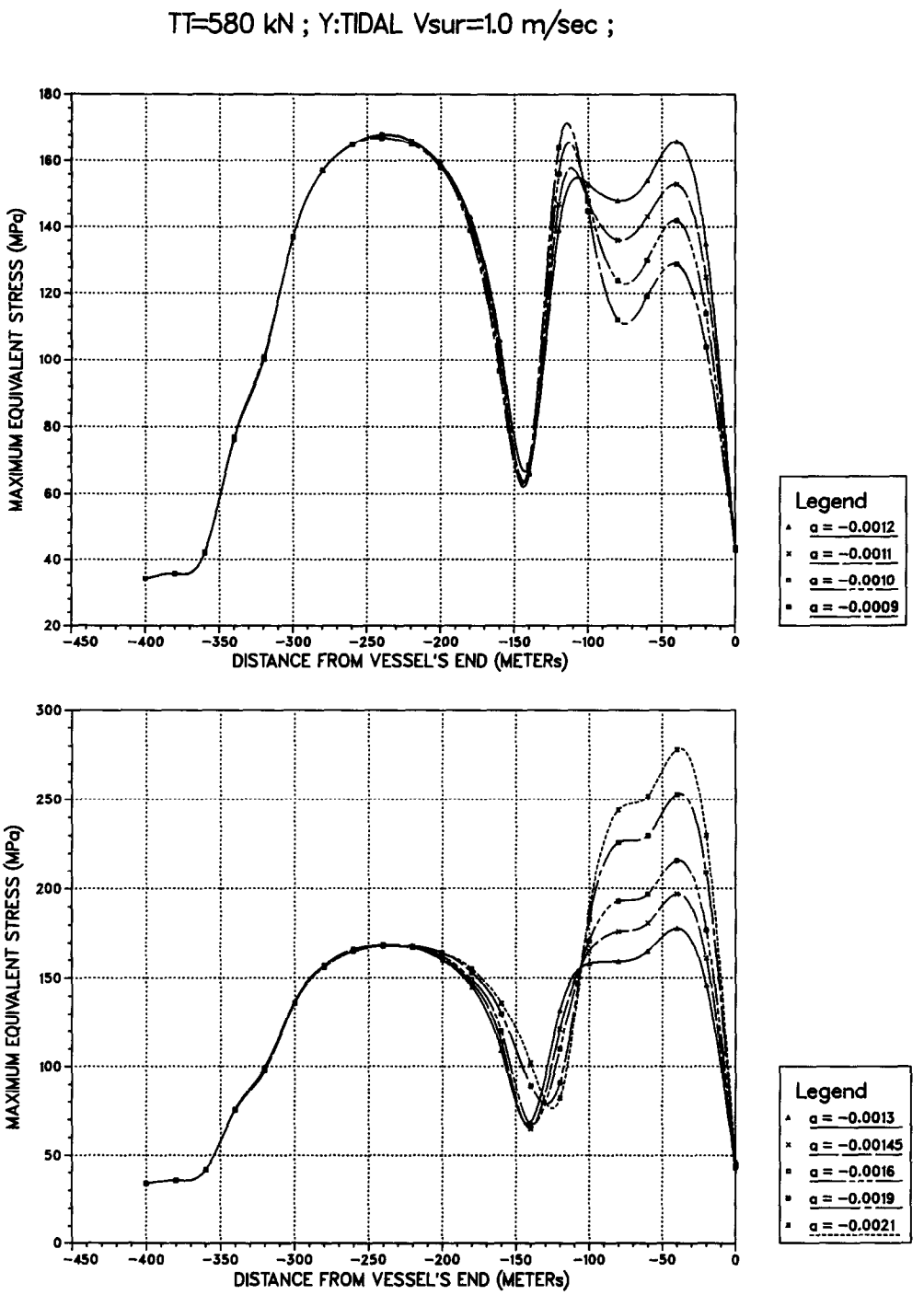

Fig. 5. Maximum equivalent stress for three-dimensional water depth; nine stinger configurations.

(vii) J-type pipelaying may be preferable to stinger laying in deep water, since the former results in reduced stresses. This can be concluded by comparing Figs 7 and 9 to 11 and 12, respectively.

(viii) In J-type pipelaying, the maximum equivalent stress graph exhibits only one maximum along the unsupported pipeline section. This is so, because there is no inflection point in the pipeline deformation. In stinger pipelaying there is a reversal in the curvature sign because of the stinger configuration.

5. SUMMARY

The static problem of pipelaying has been studied by developing a numerical solution. The pipeline model is three-dimensional, nonlinear, and has large

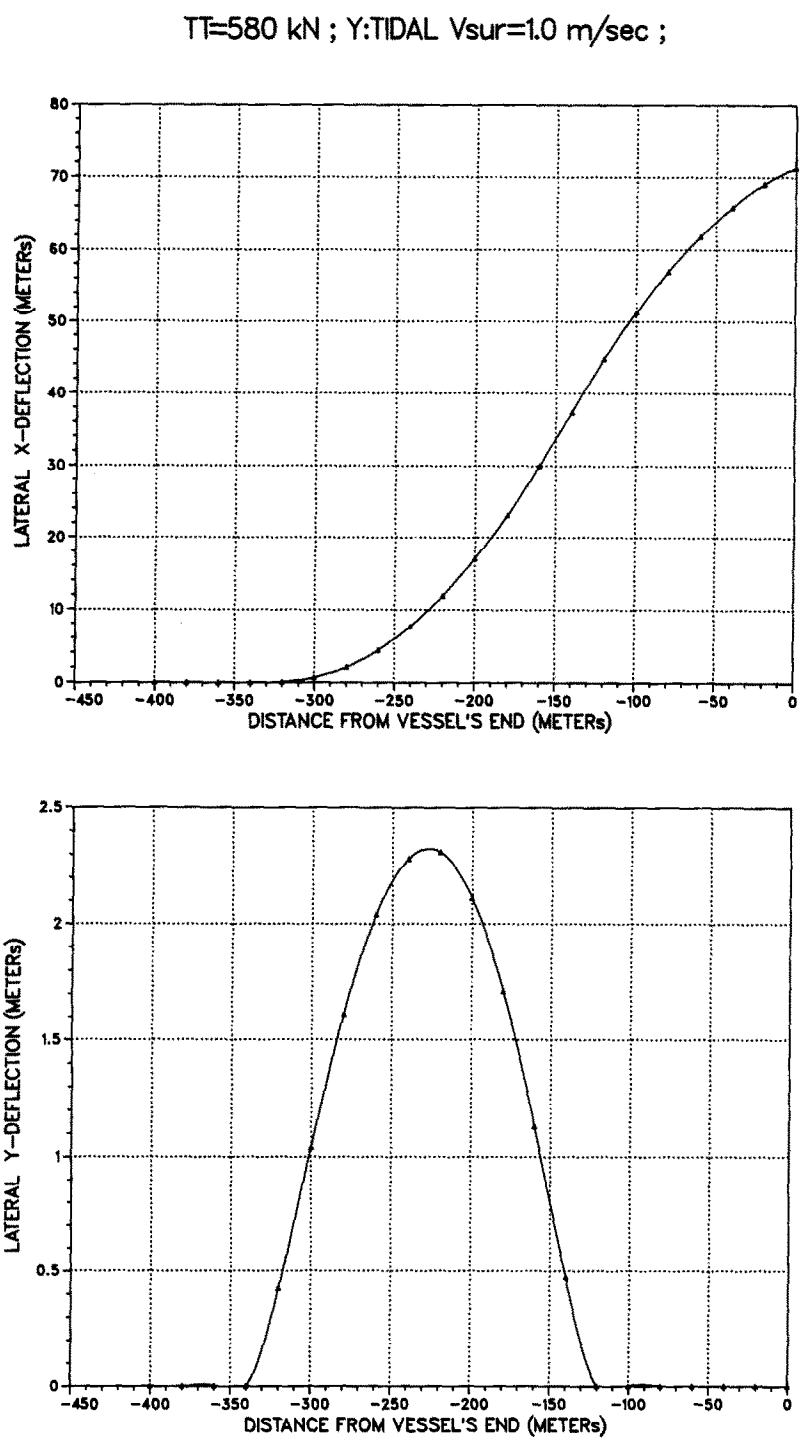

Fig. 6. Lateral x- and y-deflections for three-dimensional pipelaying in 67 m water depth; stinger configuration $a = -0.0012$.

deformation. The nonpenetration, nonadhesion and friction constraints have been used to model the seabed and stinger constraints and to identify the constrained degrees of freedom. The latter are used in a condensation process to produce a reduced matrix problem which is used to compute reaction forces. An incremental finite element method has been used for space integration to handle the nonlinearities of the model. The deformation dependent hydrodynamic load and all stiffness matrices are updated within each increment. All three aspects of the developed algorithm, that is, the incremental finite element technique, the contact constraints, and the condensation process, have been thoroughly tested by studying simple

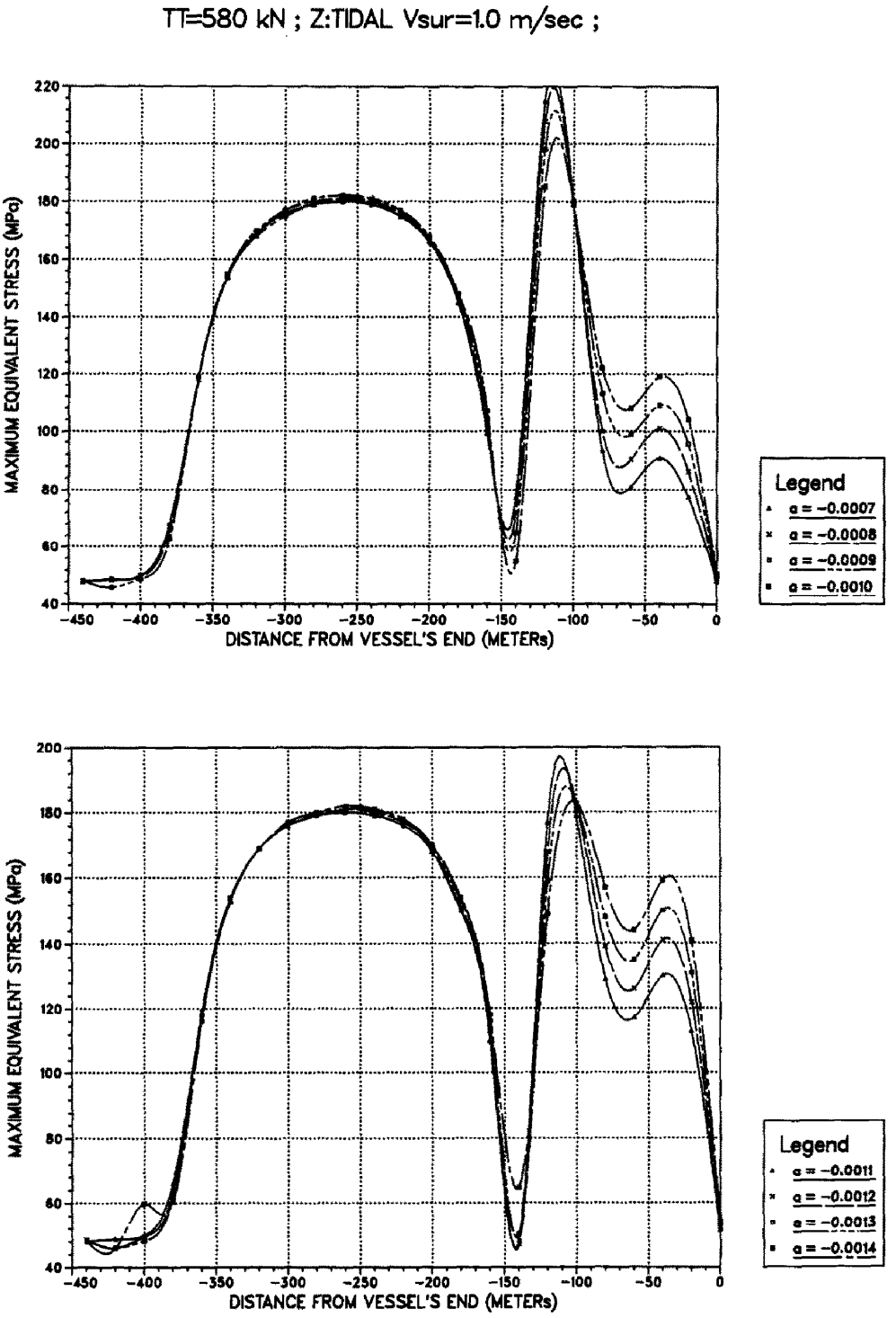

Fig. 7. Maximum equivalent stress for two-dimensional pipelaying in 125 m water depth; eight stinger configurations.

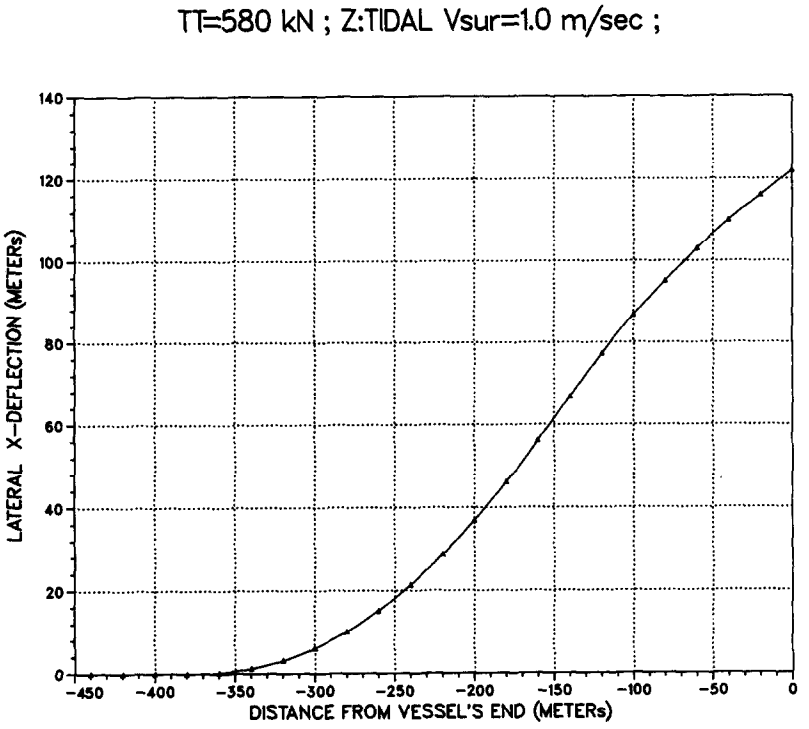

Fig. 8. Inplane pipeline deflection for two-dimensional pipelaying in 125 m water depth; stinger configuration $a = -0.0011$.

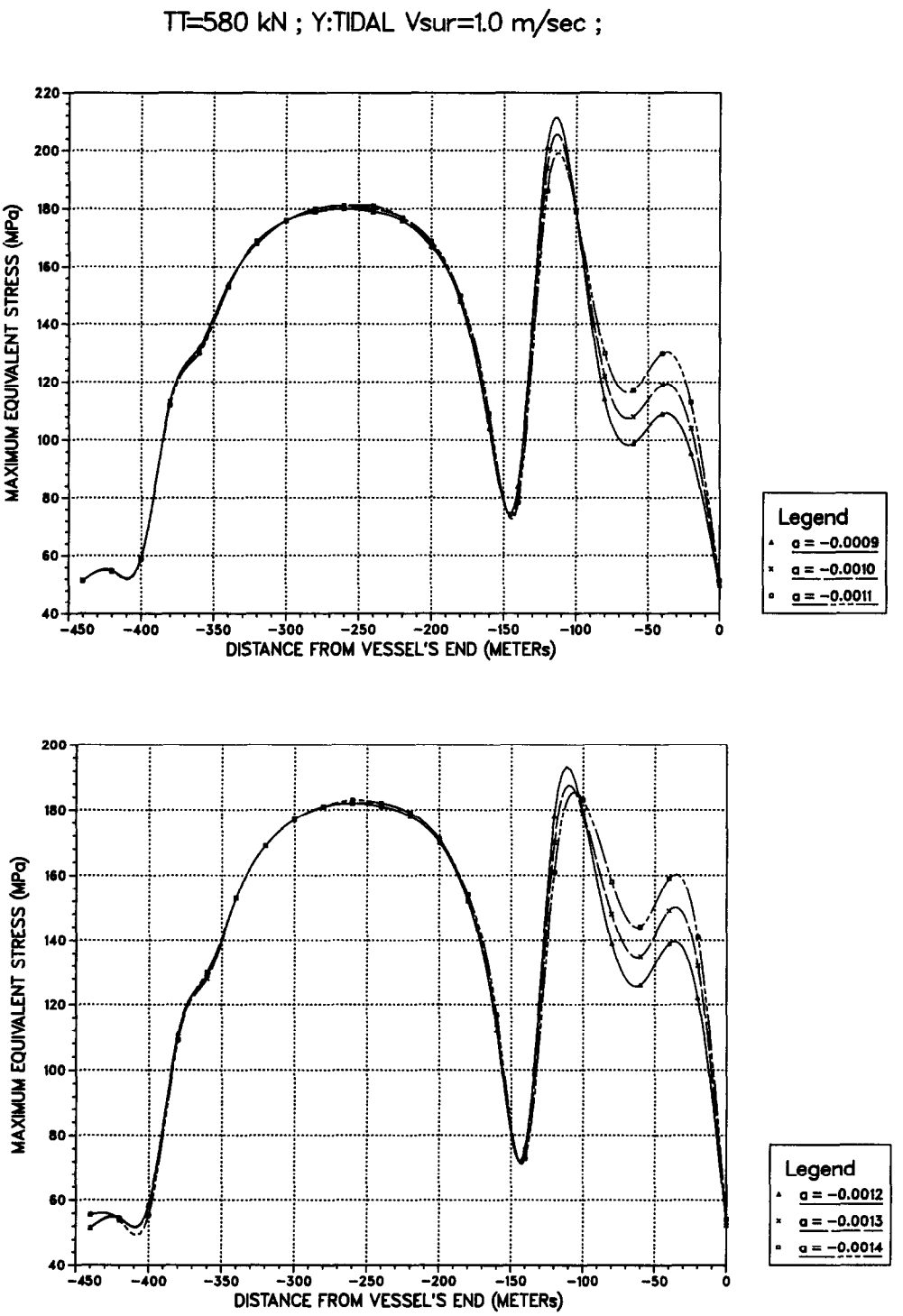

Fig. 9. Maximum equivalent stress for three-dimensional pipelaying in 125 m water depth; six stinger configurations.

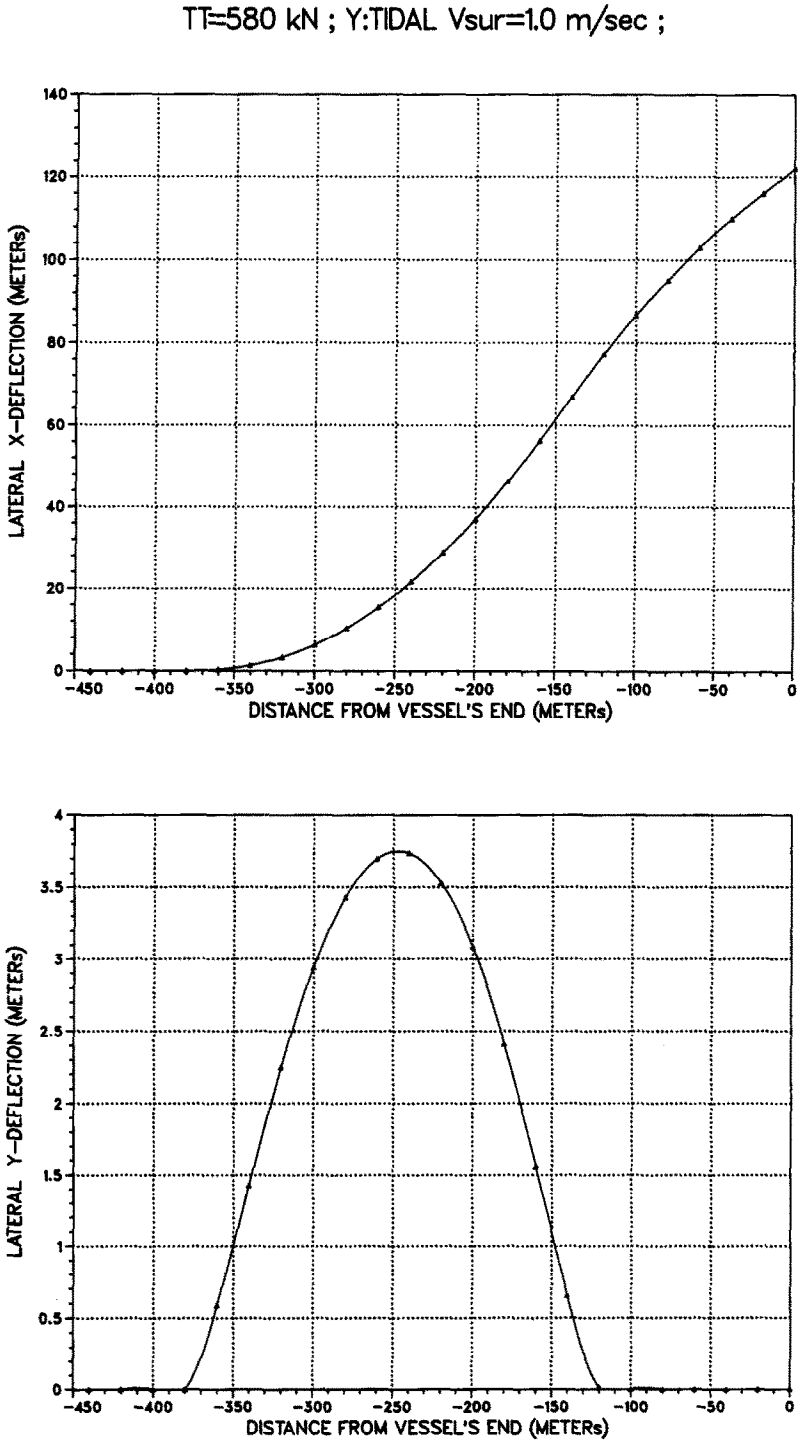

Fig. 10. Lateral x- and y-deflections for three-dimensional pipelaying in 125 m water depth; stinger configuration $a = -0.0011$.

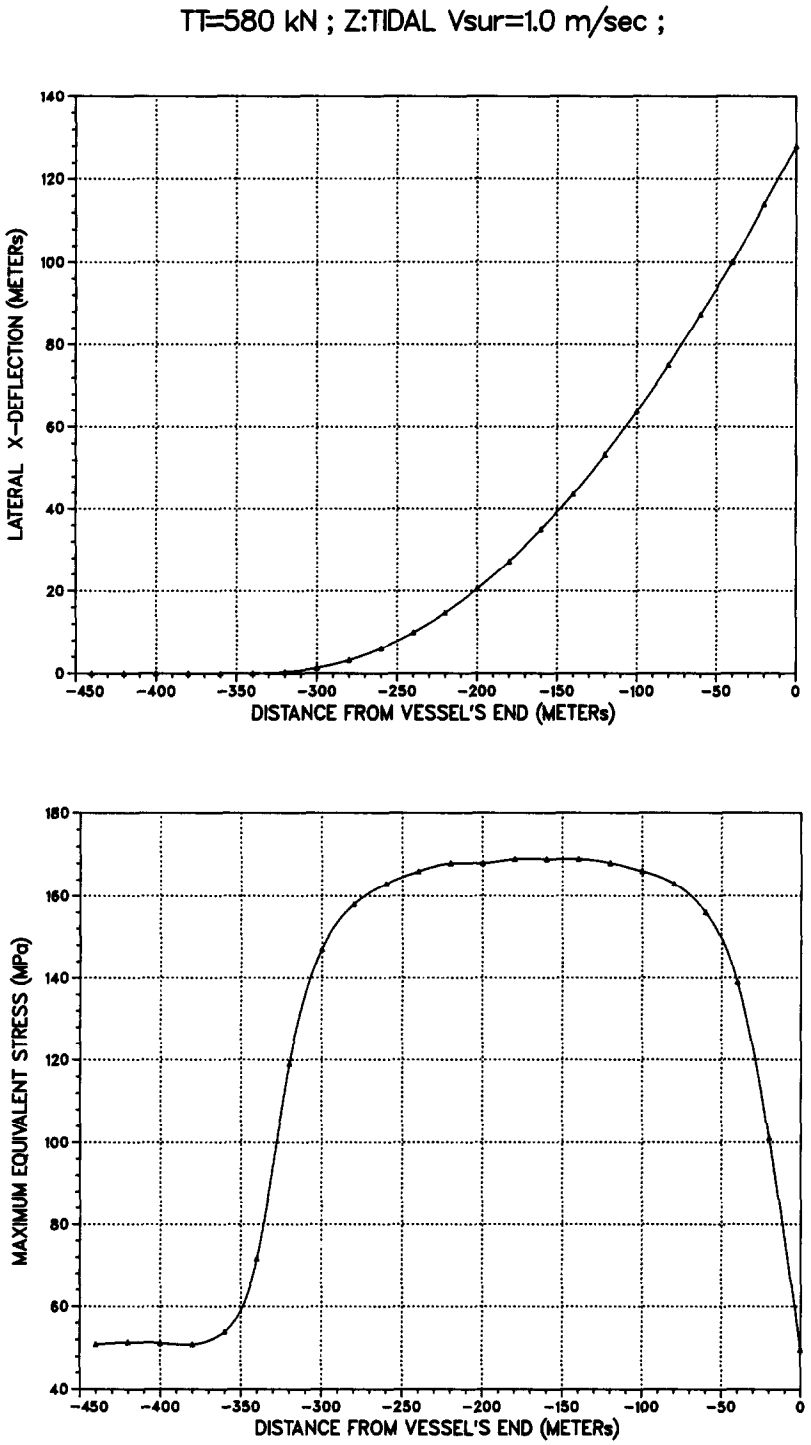

Fig. 11. Inplane pipeline deflection and maximum equivalent stress for two-dimensional pipelaying in 125 m water depth.

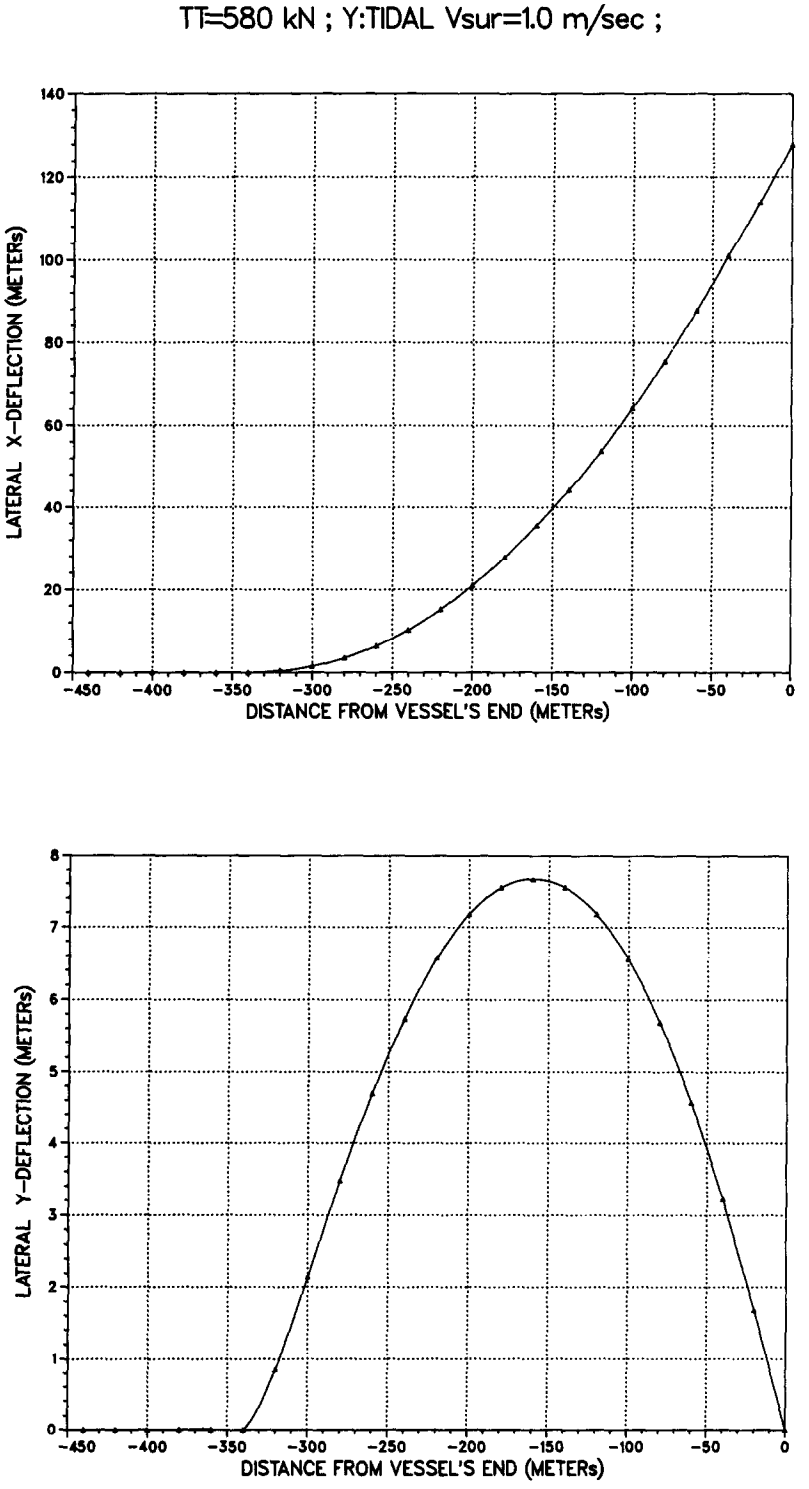
TT=580 kN ; Y:TIDAL Vsur=1.0 m/sec ;
LATERAL X-DEFLECTION (METERs)
140
120
100
80
60
40
20
0
-450 -400 -350 -300 -250 -200 -150 -100 -50 0
DISTANCE FROM VESSEL'S END (METERs)
LATERAL Y-DEFLECTION (METERs)
8
7
6
5
4
3
2
1
0
-450 -400 -350 -300 -250 -200 -150 -100 -50 0
DISTANCE FROM VESSEL'S END (METERs)

Fig. 12

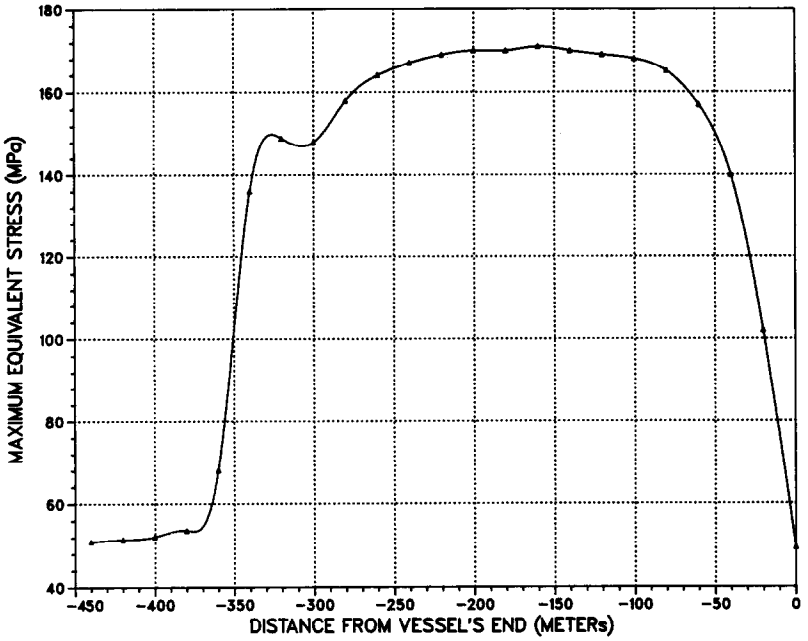

Fig. 12. Lateral x- and y-deflections and maximum equivalent stress for three-dimensional J-type pipelaying in 125 m water depth.

verification cases and other related applications on marine risers. Several practical applications have been studied numerically for both stinger and J-type pipelaying and useful conclusions have been derived.

Acknowledgements—This study has been partially sponsored by The University of Michigan/Sea Grant/Industry Consortium in Offshore Engineering under Michigan Sea Grant College Program, project numbers E/GLE-14 and R/T-23, under grant number NA85AA-D-SGO45C from the Office of Sea Grant, National Oceanic and Atmospheric Administration (NOAA), U.S. Department of Commerce, and funds from the State of Michigan. Industry participants include ARCO Oil and Gas Company; the American Bureau of Shipping; Conoco, Inc.; Exxon Production Research; Friede and Goldman, Ltd; Noble, Denton & Associates, Inc.; Shell Companies Foundation (1985–1986); and the U.S. Coast Guard.

REFERENCES

1. J. T. Powers and L. D. Finn, Stress analysis of offshore pipelines during installation. Proceedings of Offshore Technology Conference, Houston, TX, OTC Paper 1071, Vol. II, pp. 9–22 (1969).
2. D. Bynum Jr, *Practical Drilling Production Design*. Penn Well (1982).
3. B. Ovunc and H. Mallareddy, Stress analysis of offshore pipelines. Proceedings of Offshore Technology Conference, Houston, TX, OTC Paper 1222, Vol. 1, pp. 727–734 (1970).
4. J. R. Wilkins, Offshore pipeline stress analysis. Proceedings of Offshore Technology Conference, Houston, TX, OTC Paper 1227, Vol. 2, pp. 11–20 (1970).
5. E. Gnone, P. Signorelli and V. Giuliano, Three dimensional static and dynamic analysis of deep water sealines and risers. Proceedings of Offshore Technology Conference, Houston, TX, OTC Paper 2326, pp. 799–812 (1975).
6. E. Gnone, A. Della Greca and G. Bombassei, Experimental and theoretical data correlation of sealines during laying. Proceedings of Offshore Technology Conference, Houston, TX, OTC Paper 2599, pp. 779–793 (1976).
7. C. M. Larsen and D. Kavlie, Nonlinear analysis of oil pipelines by potential minimization. *Comput. Struct.* **8**, 733–743 (1978).
8. J. Konuk, Application of an adaptive numerical technique to 3-D pipeline problems with strong nonlinearities. *Trans. ASME, J. Energy Resources Technol.* **104**, 58–62 (1982).
9. N. Suzuki and N. Jingu, Dynamic behavior of submarine pipelines under laying operation. *Trans. ASME, J. Energy Resources Technol.* **104**, 313–318 (1982).
10. M. B. Bryndum, R. S. Colquhoun and A. Verway, Dynamic lay stresses for pipelines. Proceedings of Offshore Technology Conference, Houston, TX, OTC Paper 4267, pp. 469–478 (1982).
11. J. Oliver and E. Onate, A finite element formulation for the analysis of marine pipelines during laying operations. *J. Pipelines* **5**, 15–35 (1985).
12. M. M. Bernitsas, J. E. Kokarakis and A. Imron, Large deformation three-dimensional static analysis of deep water marine risers. *J. appl. Ocean Res.* **7**, 178–187 (1985).
13. J. E. Kokarakis and M. M. Bernitsas, Effect of extensibility on large deformation three-dimensional static behaviour of beams. *Int. J. Struct. Machines* **15**, 209–231 (1987).
14. L. E. Borgman, Computation of the ocean-wave forces on inclined cylinders. *Trans. Am. Geophys. Union* **39** (1958).
15. S. K. Chakrabarti, W. A. Tam and A. L. Wolber, Wave forces on a randomly oriented tube. Proceedings of Offshore Technology Conference, OTC Paper 2190, pp. 433–447 (1975).
16. T. J. R. Hughes, R. L. Taylor, J. L. Sackman, A. Cernier and W. Kanoknukulchai, A finite element method for a class of contact–impact problems. *Comput. Meth. appl. Mech. Engng* **8**, 249–276 (1976).

17. D. Talaslidis and P. D. Panagiotopoulos, A linear analysis approach to the solution of certain classes of variational inequality problems in structural analysis. *Int. J. Solids Struct.* **16,** 991–1005 (1980).
18. F. F. Mahmoud, N. J. Salamon and W. R. Marks, A direct automated procedure for frictionless contact problems. *Int. J. Numer. Meth. Engng* **18,** 245–257 (1982).
19. E. Stein and P. Wriggers, Stability of rods with unilateral constraints, a finite element solution. *Comput. Struct.* **19,** 205–211 (1984).
20. G. Yagawa and H. Hirayama, A finite element method for contact problems related to fracture mechanics. *Int. J. Numer. Meth. Engng* **20,** 2175–2195 (1984).
21. R. J. Gu, moving finite element analysis for the elastic beams in contact problems. *Comput. Struct.* **24,** 571–579 (1986).
22. C. Z. Karacostas, C. C. Baniotopoulos and P. D. Panagiotopoulos, Sea bed–structure interaction for submarine cables. *Comput. Struct.* **22,** 213–224 (1986).
23. M. M. Bernitsas and N. Vlahopoulos, Static nonlinear three-dimensional analysis of riser bundle by a substructuring and incremental finite element algorithm. *Int. J. Numer. Meth. Engng* **28,** 2517–2540 (1989).
24. N. Vlahopoulos, Constrained problems in riser and pipeline mechanics. Ph.D. Dissertation, Department of Naval Architecture and Marine Engineering, The University of Michigan, MI (1989).